*Graphical Abstract

Effects of graphene concentration, relative density and cellular morphology on the thermal conductivity of polycarbonate-graphene nanocomposite foams

G. Gedler, M. Antunes, T. Borca-Tasciuc, J.I. Velasco and R. Ozisik

Graphical abstract

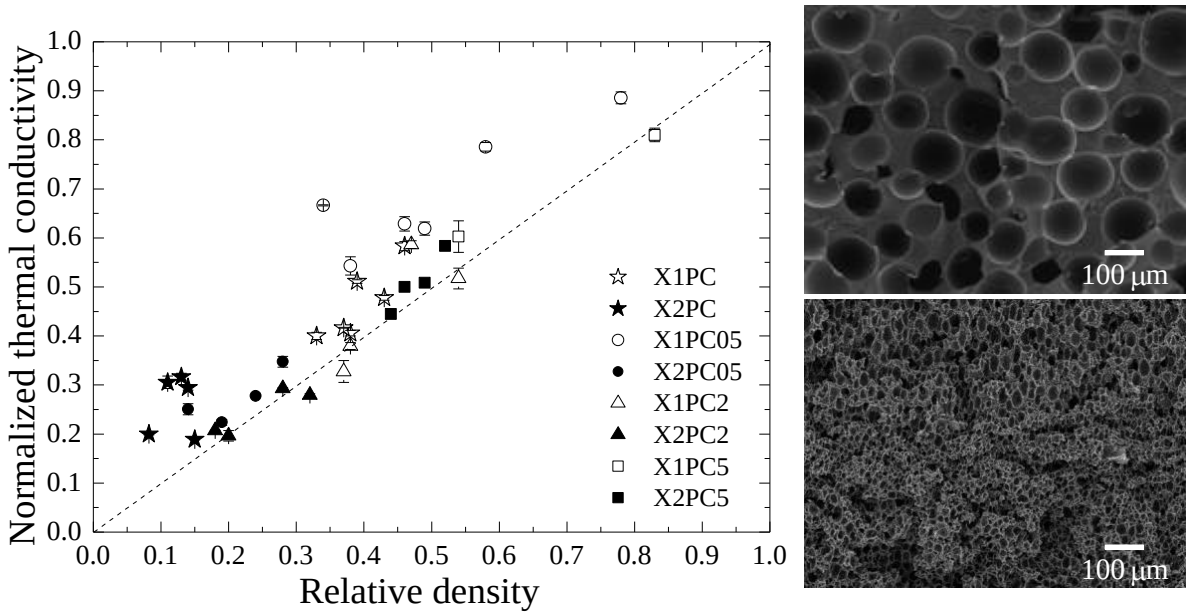

Highlights

- Polycarbonate-graphene foams were prepared via 1– and 2–step $scCO_2$ foaming
- Thermal conductivity of foams increased linearly with augmenting relative density
- Foams prepared via 1–step displayed higher thermal conductivities than 2–step foams
- The addition of higher GnP amounts led to foams with higher thermal conductivities
- GnP's effect in enhancing conductivity was less marked with increasing its content

Effects of graphene concentration, relative density and cellular morphology on the thermal conductivity of polycarbonate-graphene nanocomposite foams

G. Gedler,[a,b] M. Antunes,[a] T. Borca-Tasciuc, [c] J.I. Velasco,[a*] R. Ozisik[b,d*]

[a]Centre Català del Plàstic, Departament de Ciència dels Materials i Enginyeria Metal·lúrgica, Universitat Politècnica de Catalunya (UPC-BarcelonaTech). C/Colom 114, E-08222, Terrassa, Spain.

[b]Department of Materials Science and Engineering, [c]Department of Mechanical, Aerospace, and Nuclear Engineering, [d]Rensselaer Nanotechnology Center; Rensselaer Polytechnic Institute, Troy, NY 12180, U.S.A.

[*]Corresponding authors: jose.ignacio.velasco@upc.edu (J.I. Velasco), ozisik@rpi.edu (R. Ozisik)

Abstract

The thermal conductivity of polycarbonate-graphene nanocomposite foams was studied as a function of relative density, developed cellular structure and graphene concentration. Two types of supercritical CO_2 foaming processes were employed to obtain foams with a wide range of relative densities and cellular morphologies. The thermal conductivity of unfoamed nanocomposites increased in more than two times upon addition of 5 wt% graphene. Foaming led to lowered thermal conductivity values, as low as 0.03 W/(m·K), with thermal conductivity being mainly controlled by relative density and in a lower extent by graphene concentration. Higher thermal conductivities were obtained with increasing relative density and cell size, as well as with increasing graphene concentration, especially in those cases where improved graphene dispersion was achieved with foaming. Thermal conductivity values displayed a better fit when using a three-phase model when compared to the two-phase model previously proposed for polymer composite foams.

Keywords: *Thermal conductivity; polycarbonate; graphene; nanocomposite foams*

1. Introduction

Polymers are well known for being materials that are intrinsically thermally and electrically insulating [1-2]. As foaming further enhances the insulating behaviour of polymers by means of incorporating an important void fraction, the study of the heat transfer of polymer foams has become one of their most important fields of research, backed up by the vast number of applications and uses that these materials offer as thermal insulators [3-4]. However, many applications could benefit from the use of polymers with enhanced thermal conductivity, as for instance when used as heat sinks in electric or electronic systems [5] and in electrical wires for heat dissipation [6]. Besides the use of conductive polymers, which are expensive and commonly display a relatively low thermal stability and poor mechanical performance, the thermal conductivity of insulating polymers has been traditionally enhanced by the addition of thermally conductive fillers, including graphite, carbon black, carbon fibres, ceramic or metal particles [7-9].

Previous studies have shown that the thermal conductivity enhancement due to the addition of conductive nanofillers differs depending on the type of nanofiller and polymer matrix [9-12]. Therefore the selection of the type of filler is crucial. It has been stated that significant scatter of data are typically reported for thermal conductivity of fillers. This is caused by several factors including filler purity, crystallinity, particle size and measurement method [9]. Among conductive nanofillers, graphene nanoplatelets have been recently considered to enhance the thermal conductivity of polymers [13-14]. Despite the intrinsically high thermal conductivity of graphene nanoplatelets, the thermal conductivity enhancement in polymers has been shown to be quite limited, even at high graphene volume fractions [15].

Most of the studies published regarding the heat conduction of polymer composites with carbon-based nanoparticles and particularly graphene nanoplatelets have considered the use of theoretical models [15-16], as it has been the case for unfilled polymer foams [17-20]. Efforts to enhance the thermal conductivity of polymers, especially thermoset-based, by means of adding conductive carbon nanoparticles have been reported [21-28]. It has been shown that the addition of graphite or graphene-like nanoplatelets to epoxy results in linear increases in thermal conductivity with increasing nanoparticles concentration, reaching enhancements of four times the thermal conductivity of unfilled epoxy with adding 5 wt% graphene or as high as twenty times at 40 wt% graphene loading [21]. Similarly, the formation of strong interfacial interactions

between matrix and nanoparticle, for instance by means of silane-crosslinking, has been shown to enhance thermal conductivity [23-28].

Scarce experimental work has been dedicated to the study of the thermal conductivity of polymer foams containing carbon-based nanoparticles. In one of our works we studied the thermal conductivity behavior of polypropylene-carbon nanofibres (PP-CNF) composite foams [29]. It was found that carbon nanofibres were not efficient in increasing the thermal conductivity of PP-based foams, its value resulting almost constant and independent of CNF's volume fraction, which was related to the possible partial rupture, poor dispersion and aggregation of CNFs during processing, limiting the possibility of intimate contact between the nanofibres, crucial to attain significant thermal conductivity improvements [30]. Similarly, Shen et al. [31] demonstrated that for PS-CNF nanocomposite foams the addition of increasingly higher concentrations of CNFs only slightly enhanced the thermal conductivity, which was related to the presence of insulating polymer between the conductive nanofibres, limiting thermal conduction. In the same way, Zheng and co-workers [32-33] have recently demonstrated that the thermal conductivity of microcellular polyetherimide-graphene nanocomposite foams tends to decrease gradually with reducing cell size, reaching values as low as 0.036 W/(m·K) even for GnP contents as high as 7 wt%, typical of thermally insulating polymer foams. Authors showed that these low thermal conductivities were due on the one hand to the fact that it was not possible to establish a thermally conductive network by physical contact between the graphene nanoplatelets and, on the other, carbon-based graphene acted as IR absorber and reflector, reducing thermal radiation.

Due to the lack of studies regarding the thermal conductivity behavior of polymer nanocomposite foams based on polycarbonate (PC), which is one of the most used thermoplastic polymers in electric and electronic applications, in the current study we investigate the effects of foaming process variables, the resulting cellular morphology and graphene nanoplatelet concentration of PC-graphene nanocomposite foams on their thermal conductivity.

2. Experimental

2.1. Materials and compounding

Polycarbonate used in the current study (Lexan 123R, SABIC; Sittard, Netherlands) has a density of 1.2 g/cm^3 and a melt flow index (MFI) of 17.5 g/10 min measured at 300 ºC and 1.2 kg according to ISO 1133. Graphene nanoplatelets (GnP; XG Sciences, Inc.; Michigan, U.S.A.) had 6 to 8 nm thickness with a 15 μm average platelet lateral dimension and a bulk density of 2.2 g/cm^3, as reported by the manufacturer. PC-GnP nanocomposites containing 0.5, 2 and 5 wt% GnP, respectively named for now on PC05, PC2 and PC5, were prepared by melt-mixing using a Brabender Plasti-Corder internal mixer followed by compression moulding, as explained in our previous work [34].

2.2. Foaming

Polymer foaming processes based on the use of CO_2 as physical blowing agent have been vastly considered in both industrial and research fields [35]. Among these, batch foaming using supercritical CO_2 ($scCO_2$), where foaming can be done in both 1–step by means of sudden pressure drop at relatively high temperatures (also known as the pressure-quench method [36]) or in 2–steps where, after a first step of $scCO_2$ saturation at high pressure and low temperature, foaming is usually done by heating in a second stage the saturated CO_2-polymer sample, has been considered as a very versatile process to obtain from very low density foams with highly anisotropic cellular structures to microcellular or even nanocellular polymer foams [37-42], hence enabling the preparation of foams with a wide density range and different cellular structures.

With this in mind, two types of foaming processes were used in the current study: 1–step and 2–step foaming. In both cases, compression–moulded PC-GnP composite circular-shaped discs were saturated with supercritical CO_2 and then expanded (foamed) via $scCO_2$ dissolution. These samples are marked as "1–step" [34]. In the case of "2–step" foaming, after $scCO_2$ dissolution stage inside a high pressure vessel at 80 ºC with a total dissolution time of 210 min, discs containing CO_2 were taken out of the pressure vessel and left to stabilize at room temperature and atmospheric pressure for 120 min. Following the stabilization stage, PC-GnP circular-shaped discs saturated with CO_2 were heated under pressure in a hot-plate press IQAP LAP PL-15 at

165 ºC and 6 MPa for 40, 60, 80 or 100 seconds followed by a sudden pressure release allowing their expansion in the vertical (thickness direction) and width directions (radial direction) [43-44].

2.3. Morphology analysis

The density of the several foams was measured according to standard procedures (ISO 845), while the relative density was calculated by dividing this value by the density of the respective unfoamed material. Composite foams morphologies were analyzed using a JEOL JSM-5610 scanning electron microscope (SEM) with a voltage of 15 kV and a working distance of 30 mm. SEM samples were prepared by brittle fracturing the foams using liquid nitrogen. The resulting fracture surfaces were coated with a thin layer of gold using a BAL-TEC SCD005 Sputter Coater in argon atmosphere. The average cell size (ϕ) along the vertical direction (ϕ_{VD}) and radial direction (sample width, ϕ_{WD}) were measured using the intercept counting method [45].

For transmission electron microscopy (TEM) imaging, samples were ultramicrotomed using a PowerTome XL Ultramicrotome (Boeckeler Instruments, Inc.) in the through-plane direction to slices of approximately 60-80 nm in thickness using a diamond knife, after which samples were placed onto copper TEM grids (Ted Pella 400 mesh). TEM images were acquired using a JEOL JEM-2011 LaB6 at 200 kV with an AMT-XR280 side mount camera.

2.4. Thermal conductivity measurements

Samples used for measuring the thermal conductivity were prepared by cutting and sanding down to a diameter of 6 mm and thickness of 3 mm. The thermal conductivity was measured at room temperature using a steady state 1–dimensional heat conduction method. The experimental setup, shown in Figure 1, consisted of an electrical heater, a heat sink and two thermocouples to measure the temperature gradient across the sample thickness. To minimize the interface thermal resistance, electrically insulated thermocouples were embedded into two soft indium layers to measure the temperature at both sides of the sample. Pressure was applied using a screw mechanism that was thermally insulated from the sample by a thick poly(tetrafluoroethylene) block (insulation block). The rest of the set up was thermally insulated by a very low thermal conductivity material (≈ 0.02 W/(m·K)) in order to reduce any heat loss by convection/radiation.

Finally, a dome was placed on top of the entire setup to reduce the influence of any current of air during measurement.

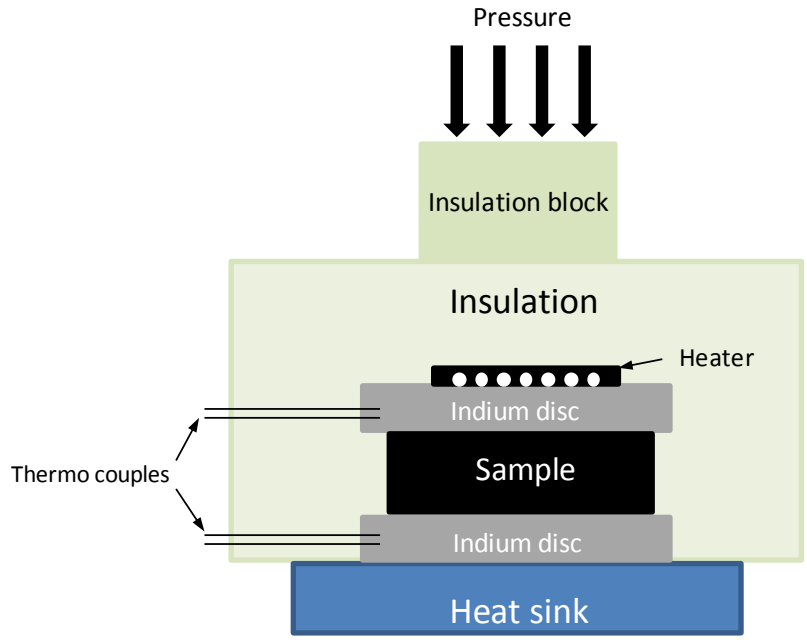

Figure 1. Scheme of the setup used for measuring thermal resistance.

The heat losses in the experimental setup were calibrated using glass samples of known conductivity, including glass wool having a calibrated thermal conductivity of 0.04 W/(m·K). To measure the thermal conductivity (k), first of all the experimental thermal resistance was obtained from the slope of the temperature difference across the sample as a function of heater power. Next, the calibrated heat loss (R_{Loss}) contribution was taken into account by using a parallel thermal resistance network arrangement. To find the intrinsic thermal conductivity, the interface thermal resistance between the composite sample and the indium layer ($R_{Interface}$) was subtracted from the overall conduction resistance (R_{Total}). This interface thermal resistance was determined by testing samples with different thicknesses and extrapolating the plot of sample and interface resistance ($R_{Sample} + R_{Interface}$) vs. sample thickness to zero thickness using linear regression. The thermal resistance (R_{Sample}) and thermal conductivity (k) were calculated using expressions (1) and (2), respectively:

$$R_{Sample} = \frac{R_{Loss} \cdot R_{Total}}{R_{Loss} - R_{Total}} - R_{Interface} \quad (1)$$

$$k = \frac{1}{R_{Sample}}\left(\frac{t}{A}\right) \quad (2)$$

where t and A are the thickness and cross sectional area of the sample, respectively. The same procedure was used for all samples. The thermal conductivity of unfoamed PC was measured to be 0.18 W/(m·K), which is very close to the values reported in literature [9, 46].

3. Results and discussion

3.1. Cellular morphology

The characteristics of the cellular structures obtained by foaming PC and PC-GnP nanocomposites via the 1– and 2–step foaming processes are presented in Table 1. Cellular morphologies were influenced by a combination of factors such as carbon dioxide dissolution/expansion process parameters, foaming method (1–step vs. 2–step), and graphene concentration. In general, samples foamed via 2–step showed lower relative densities and smaller cell sizes and, as a consequence, higher cell densities, than those foamed via 1–step. It should be noted that normally lower relative densities are more easily achievable with the generation of bigger cells during foaming [47]; however, in the current study, foams prepared via 2–step presented substantially lower relative densities and at the same time smaller cell sizes.

Addition of graphene also had a major impact on cellular morphology. In general, as graphene concentration increased, relative density also increased, and the presence of GnP led to a broader range of relative densities: $\rho_{rel,1-step}$ = 0.34–0.83 and $\rho_{rel,2-step}$ = 0.08–0.52 for PC-GnP nanocomposite foams, and $\rho_{rel,1-step}$ = 0.33–0.46 and $\rho_{rel,2-step}$ = 0.08–0.15 for unfilled PC foams (Table 1).

3.2. Thermal conductivity

The broad cellular morphologies achieved using various foaming process conditions and graphene nanoparticle concentrations strongly influenced the thermal conductivity.

Comparatively, the thermal conductivity of PC-GnP nanocomposites was greater than that of the unfilled PC, with thermal conductivity increasing with increasing graphene concentration. In addition, although foams prepared via 1– and 2–step foaming showed some overlapping thermal conductivity values, globally they were also somewhat separated from each other, which could be due to their different relative density and cellular morphology. The effects of the cellular morphology and graphene concentration on the thermal conductivity are further discussed in the following sections.

3.2.1. Influence of the cellular morphology

The cellular morphology of foams can be characterized using various parameters, and experimental measurements of four of such parameters, particularly relative density, cell density, cell size, and aspect ratio, are presented in Table 1. Relative density is one of the most widely used and recognized characteristics of foams; therefore, its effect on the thermal conductivity is presented first among all other variables in Figure 2a for unfilled unfoamed and foamed PC, alongside unfoamed and foamed PC-GnP nanocomposites. Results indicate that thermal conductivity increased with increasing relative density, with almost a linear correlation between both (Figure 2a), which suggests that the main heat transfer mechanism was conduction through the solid [3]. It has been reported that convection due to gas movement inside cells may be disregarded for cellular structures with cell sizes below 4-5 mm [17], which is the case in the current study. Therefore, it is possible to state that with decreasing relative density, i.e., with increasing gas fraction and making solid cell walls and struts thinner (see Figures 2b and 2c), phonons have a more tortuous path to travel through the solid fraction, and as a result the thermal conductivity decreases.

Figure 2a also clearly demonstrates the effect of graphene concentration, which will be discussed in detail later. As graphene concentration increased, thermal conductivity values showed a tendency to increase, particularly at the high end of relative density, as indicated by the slopes of the dashed lines presented in Figure 2a. A similar finding was reported for carbon nanofibre filled PP composite foams [29].

Finally, foams prepared via 1–step foaming displayed, on average, higher values of thermal conductivity than those foamed via 2–step foaming. This effect is strongly related to the relative densities and cellular morphologies of these two sets of samples: on average 1–step samples have

greater relative densities than 2–step samples and, as a result, they are always on the high end of the relative density values (see Figure 2).

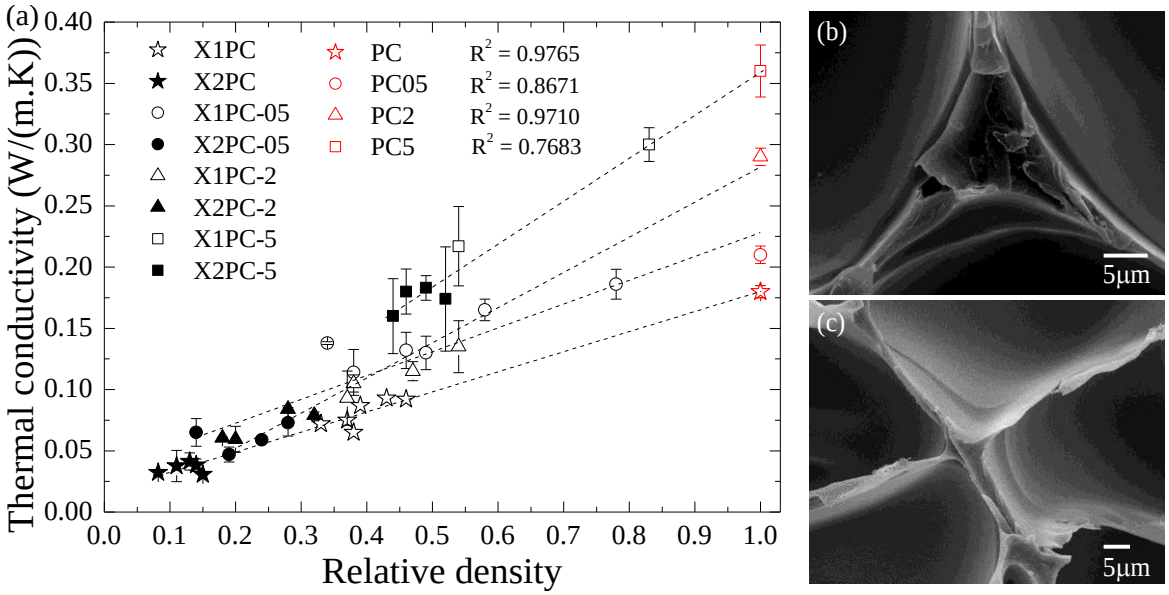

Figure 2. (a) Thermal conductivity as a function of relative density for unfoamed and foamed PC and PC-GnP nanocomposites (X1 and X2 indicate foams that were prepared by 1– and 2–step foaming, respectively). Typical SEM micrographs of the cell strut of: (b) high relative density 1–step foams and (c) low relative density 2–step foams (both with 0.5 wt% GnP). Note: R^2 values corresponding to the linear fittings are indicated for each set of foams.

In order to have a better understanding of the effects of foaming in the thermal conductivity, all thermal conductivity values (k_{foam}) were normalized by the thermal conductivity of the respective unfoamed sample ($k_{composite}$) (see Figure 3). Normalization ($k_{norm} = k_{foam}/k_{composite}$) led all samples to aggregate around a single line with a positive slope with increasing relative density, indicating that relative density is a good predictor of thermal conductivity. Additionally, as can be seen when comparing the experimental data with the dashed line shown in the figure, almost all foams presented k_{norm} values that were above the theoretical values assuming a linear relation between the normalized thermal conductivity and relative density, i.e., C =1 and n = 1 in the typical scale relation $k_{norm} = C\ (\rho_{foam}/\rho_{composite})^n$. Among these, high density 1–step foams containing 0.5 wt% GnP were the ones that displayed the highest increment, indicating their higher efficiency in enhancing thermal conductivity.

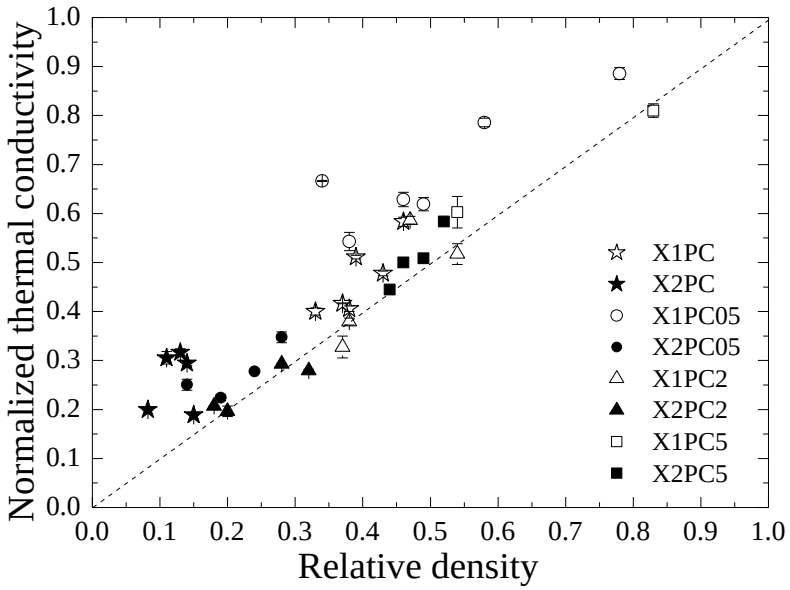

Figure 3. Normalized thermal conductivity as a function of relative density for unfilled PC and PC-GnP nanocomposite foams.

The effect of cell size on thermal conductivity is presented in Figure 4. In this case, foams prepared by 1– and 2–step foaming were clearly separated from each other. Furthermore, foams prepared via 2–step foaming showed a more pronounced deviation from each other as a function of graphene concentration, which is discussed in the following section. Interestingly, although the relationship between cell size and thermal conductivity varied strongly among different sample groups, unfilled PC foams prepared by both 1– and 2–step foaming presented a thermal conductivity behaviour that did not depend on cell size, showing constant thermal conductivities independently of cell size (evolution represented with horizontal lines), while on average the thermal conductivity of PC-GnP nanocomposite foams decreased with increasing cell size. However, this result is apparent, as within a given set of foams those having bigger cell sizes also displayed lower relative densities and, as a consequence, lower values of thermal conductivity.

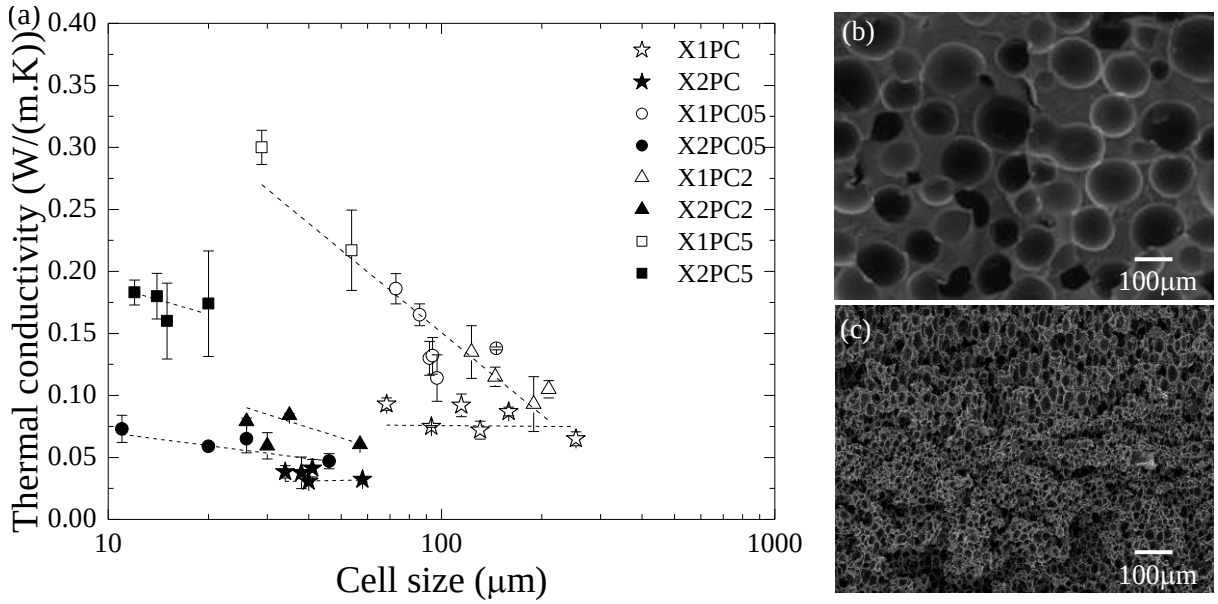

Figure 4. (a) Thermal conductivity as a function of cell size for unfilled PC and PC-GnP nanocomposite foams prepared via 1– and 2–step foaming. PC-GnP nanocomposites prepared in 1–step followed a linear behaviour while nanocomposites prepared via 2–step foaming showed a more scattered behaviour. Micrographs showing the typical cellular structure of foams prepared by: (b) 1–step (unfilled PC) and (c) 2–step foaming (5 wt% GnP).

3.2.2. Influence of graphene concentration

Although relative density is the main parameter controlling the thermal conductivity of PC-GnP nanocomposite foams, the influence of graphene concentration has to be considered, as higher GnP concentrations should lead to higher values of thermal conductivity. For this reason, it is more proper to consider the combined effects of relative density and graphene concentration on the thermal conductivity of PC-GnP nanocomposite foams by representing the thermal conductivity as a function of GnP volume concentration (Figure 5), as volume concentration takes simultaneously into account the amount of GnP present in the nanocomposite foam as well as its density. As can be seen in Figure 5, the thermal conductivity of unfoamed and foamed PC-GnP nanocomposites increased with increasing GnP volume concentration. The highest value of thermal conductivity (0.37 W/(m·K)) was achieved for the unfoamed PC-GnP nanocomposite containing around 2.7 vol% GnP (equivalent to 5 wt% GnP), about two times greater than that of unfilled PC (0.18 W/(m·K)). However, these values are much lower than expected based on the theoretical thermal conductivity of graphene nanoplatelets measured parallel to the surface

(3000 W/(m·K) [48-51]), which is related to the fact that graphene nanoparticles did not form a percolated thermally conductive network within the PC matrix.

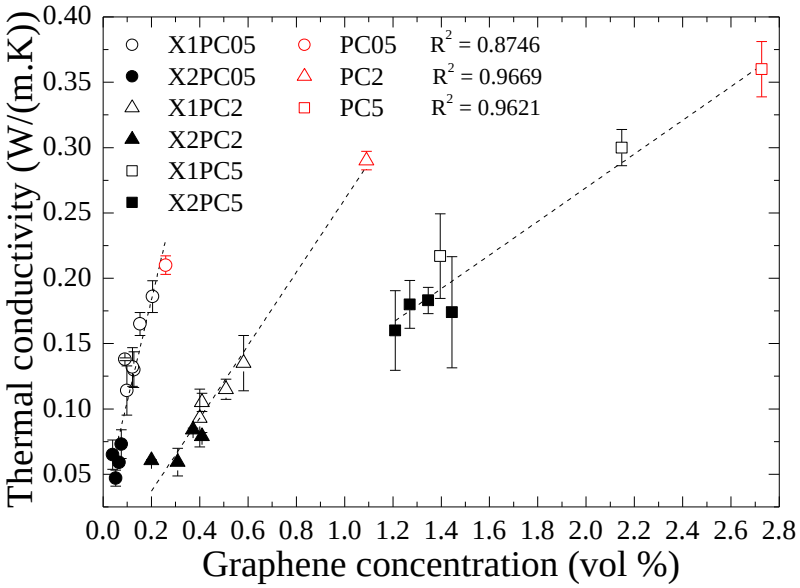

Figure 5. Thermal conductivity of PC-GnP nanocomposite foams as a function of graphene volume concentration. The thermal conductivity of unfoamed nanocomposites is indicated using red symbols. Note: R^2 values corresponding to the linear fittings are indicated for each set of foams.

Independently of the fact that the final values of thermal conductivity were much lower than expected, still the increase in thermal conductivity with increasing graphene concentration could be attributed to the following factors: (i) intrinsically high thermal conductivity of graphene, which provides a path of lower resistance for phonons; (ii) high aspect ratio of graphene nanoplatelets, which has been reported to be a possible way of enhancing the thermal conductivity of polymers [52]; and (iii) strong π–π interactions between PC molecules and graphene, which would lead to a strong interface, and phonon transfer across strong interfaces was suggested to be more efficient [53]. In addition, the influence of graphene volume concentration on the thermal conductivity resulted different for each set of foams, as increasingly higher graphene weight percentages led to smoother increments of the thermal conductivity with increasing GnP's volume concentration. Comparatively, PC-GnP foams containing 0.5 wt% GnP

presented the highest increments of thermal conductivity with increasing graphene volume concentration (steeper slope), followed by PC-GnP foams containing 2 wt% GnP and finally PC-GnP foams containing 5 wt% GnP, which could be related to the confinement of GnP nanoparticles on the solid phase of the foam (cell walls and struts), at least within the studied concentration range.

It should be pointed out that dispersion and partial exfoliation of graphene nanoplatelets may be taking place during foaming, as it has been suggested in some of our previous works that there is a direct relation between the reduction of the stacking regularity of carbon-based nanoparticles such as graphene nanoplatelets or carbon nanofibres, related to the rupture of nanoparticles aggregates and hence improved dispersion or even partial nanoparticles exfoliation, with foaming [29, 54-56]. The schematic representation displayed in Figure 6 exemplifies the suggested mechanism of dispersion/partial exfoliation of graphene nanoplatelets during foaming. As can be seen, graphene nanoplatelets act as cell nucleating sites, interacting with CO_2 molecules, which, during the expansion/foam growth stage, give way to cells, whose formation and growth help separate graphene stacks and ultimately bring graphene nanoplatelets closer through a volume exclusion effect (concentration of GnP in the foam cell walls and struts).

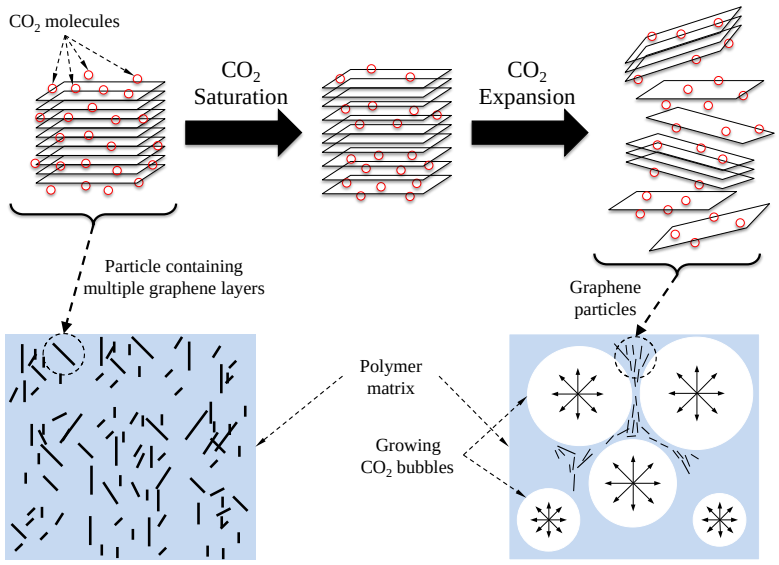

Figure 6. Scheme showing the dispersion/exfoliation of graphene nanoplatelets due to interaction with CO_2 molecules during foaming.

TEM experiments performed on PC-GnP nanocomposite foams prepared via 1–step foaming showed differences in terms of graphene nanoplatelets disposition in the foams (see Figure 7). Overall reduction of the distance between GnP particles and decreased number of layers within each particle (seen as thinner GnP nanoparticles) could be related to an enhanced GnP dispersion within the polymer, which would decrease interfacial resistance at the polymer–filler and filler–filler interfaces. In addition, a lower number of layers within each graphene particle increases the average particle aspect ratio and it has been shown that thermal conductivity can be improved with the use of high aspect ratio particles [50, 57]. It should be noted that the effect of $scCO_2$ foaming on the dispersion of GnP was found to weaken with increasing GnP concentration (see Figure 7b), as increasing the amount of GnP makes it harder to separate and disperse graphene nanoplatelets at the same foaming conditions, which could explain the thermal conductivity behaviour of PC-GnP nanocomposite foams at GnP concentrations above 0.5 wt%.

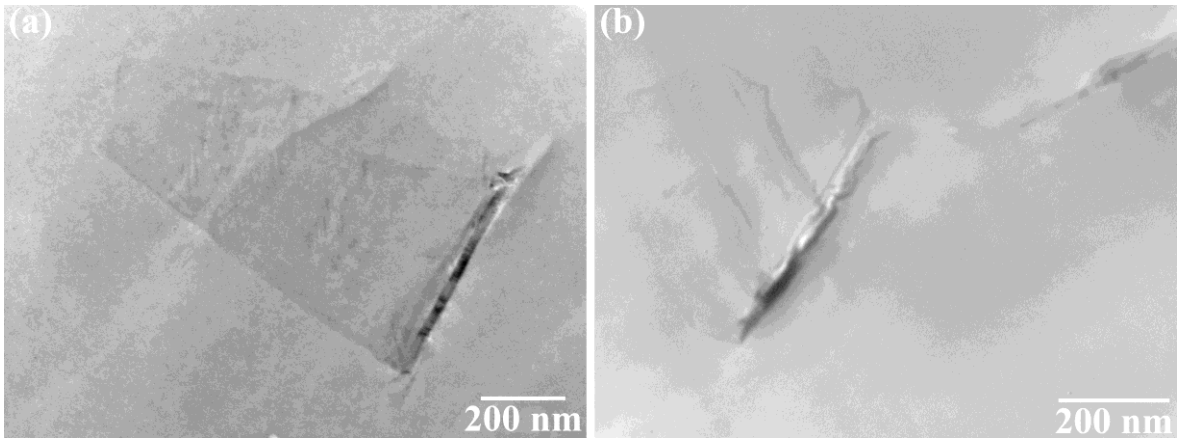

Figure 7. TEM micrographs of graphene nanoparticles present in PC-GnP nanocomposite foams prepared via 1–step foaming: (a) X1PC05 foams exhibited thinner and more close GnP nanoparticles when compared to (b) X1PC2 foams.

3.2.3. Comparison with theoretical predictions

Theoretical thermal conductivities were calculated using two different models previously proposed for polymer composite foams [29]. The first model (Model I) assumes that the system is formed by two phases: a gas phase and a composite phase (in the current study, polycarbonate with graphene), while the second model (Model II) assumes a three–phase system consisting of

gas, polymer matrix and filler. The thermal conductivities corresponding to Model I (k_I) and Model II (k_{II}) are calculated as follows:

$$k_I = k_{gas}V_{gas} + \xi\left(k_{composite}V_{composite}\right) \quad (3)$$

$$k_{II} = k_{gas}V_{gas} + \xi\left(k_{polymer}V_{polymer} + k_{filler}V_{filler}\right) \quad (4)$$

where k_{gas}, $k_{composite}$, $k_{polymer}$, and k_{filler} are the thermal conductivities of air (0.026 W/(m·K) [58]), composite (polycarbonate-graphene), polycarbonate, and graphene nanoplatelets (3000 W/(m·K) parallel to the surface, as indicated by the manufacturer), respectively; V_{gas}, $V_{composite}$, $V_{polymer}$ and V_{filler} are the corresponding volume fractions; and ξ is a parameter known as tortuosity, which is related to the complexity of the cellular structure [47].

The experimental and theoretical thermal conductivities calculated using equations (3) and (4) are compared in Figure 8 for all PC-GnP nanocomposite foams. As can be seen, the three–phase model (Model II, indicated with red symbols in Figure 8) showed a better agreement with the experimental values than the two–phase model (Model I, black symbols in Figure 8). Model I showed a strong deviation with increasing relative density and graphene concentration. This is attributed to the individual theoretical contributions of each of the phases in the nanocomposite foams taken into consideration when using Model II.

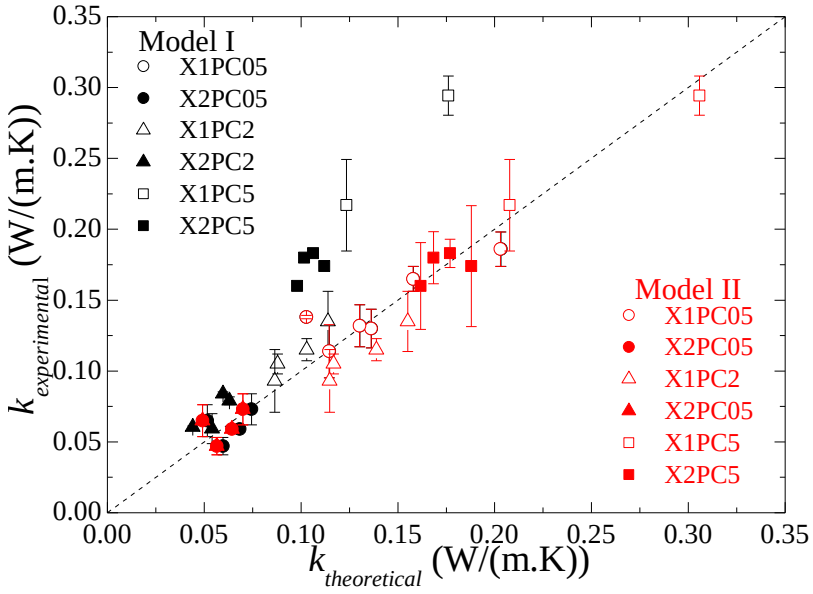

Figure 8. Comparison between the experimentally measured thermal conductivities ($k_{experimental}$) and the theoretical thermal conductivities calculated using Model I (black symbols) and Model II (red symbols) of PC-GnP nanocomposite foams.

4. Conclusions

The thermal conductivity of polycarbonate-graphene foams prepared via 1– and 2–step $scCO_2$ foaming was found to depend on both relative density and cellular morphology developed during foaming, as well as graphene concentration. Results indicate that thermal conductivity increases almost linearly with increasing relative density, suggesting that the main heat transfer was conduction through the solid phase. Comparatively, foams prepared via 1–step displayed higher thermal conductivities than those prepared using 2–step foaming, which was related to their higher relative densities and cell sizes. Although the addition of a higher amount of graphene resulted in foams with globally higher thermal conductivities, it was observed that its effect was less pronounced with increasing graphene concentration, which was explained by the confinement of GnP nanoparticles on the solid phase of the foams. Theoretical calculations showed that the use of a three-phase model that takes into account the separate contribution of the gas phase, polymer phase and filler phase to calculate the thermal conductivity fits better to the experimental values, hence being more appropriate to estimate the thermal conductivity of polymer nanocomposite foams.

As the maximum reached thermal conductivity for PC-GnP nanocomposite foams was still quite low and characteristic of thermally-insulating materials, future work should focus on favouring heat conduction through the material. As the heat transfer mechanism requires an intimate contact between conductive nanoparticles, depending on, besides nanoparticles morphology aspects, the interphase between polymer and carbon nanoparticles, as the presence of insulating matrix or even polymer crystal domains between nanoparticles would result in highly resistive thermal junctions [56], strategies should be used in order to guarantee physical contact between nanoparticles. On the one hand, dispersion and, in the case of graphene nanoplatelets, full nanoplatelet exfoliation, should be attained, possibly by means of using a proper combination of high-shear melt-mixing and selected foaming parameters; on the other hand, as dispersion is improved, contact between the dispersed nanoparticles has to be guaranteed, meaning that the level of foaming (density reduction and developed cellular structure) has to be properly controlled in order to form a proper conductive path throughout the cell walls without any type of disruption.

Acknowledgements

The authors would like to acknowledge the Spanish Ministry of Economy and Competitiveness for the financial support of project MAT2014-56213, the National Science Foundation (CMMI–1200270 and 1538730, DUE–1003574 and 1406405). T.B.T. gratefully acknowledges funding from the U.S. Department of Energy, Office of Science, and Office of Basic Energy Sciences through the S3TEC Energy Frontiers Research Center at MIT under Award No. DE-SC0001299.

References

[1] Y. Agari, T. Uno, Thermal conductivity of polymer filled with carbon materials: Effect of conductive particle chains on thermal conductivity, J. Appl. Polym. Sci. 30 (1985) 2225-2235.

[2] J.A. King, K.W. Tucker, J.D. Meyers, E.H. Weber, M.L. Clingerman, K.R. Ambrosius, Factorial design approach applied to electrically and thermally conductive nylon 6,6, Polym. Comp. 22 (2001) 142-154.

[3] M. Antunes, J.I. Velasco, E. Solórzano, M.A. Rodríguez-Pérez, Heat transfer in polyolefin foams. In: Oechsner A., Murch G.E., eds. Heat Transfer in Multi-Phase Materials. Berlin: Springer-Verlag Berlin Heidelberg, 2011, p. 131-162.

[4] B. Wicklein, A. Kocjan, G. Salazar-Alvarez, F. Carosio, G. Camino, M. Antonietti, et al., Thermally insulating and fire-retardant lightweight anisotropic foams based on nanocellulose and graphene oxide, Nat. Nano. 10 (2015) 277-283.

[5] J.A. King, K.W. Tucker, B.D. Vogt, E.H. Weber, C. Quan, Electrically and thermally conductive nylon 6,6, Polym. Comp. 20 (1999) 643-654.

[6] R. Verdejo, F. Barroso-Bujans, M.A. Rodríguez-Pérez, J.A. de Saja, M.A. López-Manchado, Functionalized graphene sheet filled silicone foam nanocomposites, J. Mater. Chem. 18 (2008) 2221-2226.

[7] Wolff S., Wang M. Carbon black science & technology. 2nd ed. New York: CRC Press, 1993.

[8] K. Pashayi, H.R. Fard, F. Lai, S. Iruvanti, J. Plawsky, T. Borca-Tasciuc, Self-constructed tree-shape high thermal conductivity nanosilver networks in epoxy, Nanoscale. 6 (2014) 4292-4296.

[9] Z. Han, A. Fina, Thermal conductivity of carbon nanotubes and their polymer nanocomposites: A review, Prog. Polym. Sci. 36 (2011) 914-944.

[10] Wypych G. Handbook of fillers: physical properties of fillers and filled materials. Toronto: ChemTec Publishing, 2000.

[11] J.E. Fischer, Carbon nanotubes: structure and properties. In: Gogotsi Y, ed. Carbon nanomaterials. New York: Taylor and Francis Group, 2006, p. 51-58.

[12] K. Hu, D.D. Kulkarni, I. Choi, V.V. Tsukruk, Graphene-polymer nanocomposites for structural and functional applications, Prog. Polym. Sci. 39 (2014) 1934-1972.

[13] H. Fukushima, L.T. Drzal, B.P. Rook, M.J. Rich, Thermal conductivity of exfoliated graphite nanocomposites, J. Ther. Anal. Calorim. 85 (2006) 235-238.

[14] X. Jiang, L.T. Drzal, Multifunctional high density polyethylene nanocomposites produced by incorporation of exfoliated graphite nanoplatelets 1: Morphology and mechanical properties, Polym. Comp. 31 (2010) 1091-1098.

[15] L. Hu, T. Desai, P. Keblinski, Thermal transport in graphene-based nanocomposite, J. Appl. Phys. 110 (2011) 033517.

[16] K. Chu, C.-C. Jia, W.-S. Li, Effective thermal conductivity of graphene-based composites, Appl. Phys. Lett. 101 (2012) 121916.

[17] L. Glicksman, Heat transfer in foams. In: Hilyard N.C., Cunningham A., eds. Low density cellular plastics. Netherlands: Springer, 1994, p. 104-152.

[18] M. Gustavsson, E. Karawacki, S.E. Gustafsson, Thermal conductivity, thermal diffusivity, and specific heat of thin samples from transient measurements with hot disk sensors, Rev. Sci. Inst. 65 (1994) 3856-3859.

[19] R. Coquard, D. Baillis, Numerical investigation of conductive heat transfer in high-porosity foams, Acta Mater. 57 (2009) 5466-5479.

[20] A. Ahern, G. Verbist, D. Weaire, R. Phelan, H. Fleurent, The conductivity of foams: a generalisation of the electrical to the thermal case, Coll. Surf. A: Physicochem. Eng. Asp. 263 (2005) 275-279.

[21] A. Yu, P. Ramesh, X. Sun, E. Bekyarova, M.E. Itkis, R.C. Haddon, Enhanced thermal conductivity in a hybrid graphite nanoplatelet – carbon nanotube filler for epoxy composites, Adv. Mater. 20 (2008) 4740-4744.

[22] L.M. Veca, M.J. Meziani, W. Wang, X. Wang, F. Lu, P. Zhang, Y. Lin, R. Fee, J.W. Connell, Y.P. Sun, Carbon nanosheets for polymeric nanocomposites with high thermal conductivity, Adv. Mater. 21 (2009) 2088-2092.

[23] W.S. Ma, J. Li, X.S. Zhao, Improving the thermal and mechanical properties of silicone polymer by incorporating functionalized graphene oxide, J. Mater. Sci. 48 (2013) 5287-5294.

[24] H.K.F. Cheng, T. Basu, N.G. Sahoo, L. Li, S.H. Chan, Current advances in the carbon nanotube/thermotropic main-chain liquid crystalline polymer nanocomposites and their blends, Polymers 4 (2012) 889-912.

[25] M.C. Hsiao, C.C.M. Ma, J.C. Chiang, K.K. Ho, T.Y. Chou, X. Xie, C.H. Tsai, L.H. Chang, C.K. Hsieh, Thermally conductive and electrically insulating epoxy nanocomposites with thermally reduced graphene oxide-silica hybrid nanosheets, Nanoscale 5 (2013) 5863-5871.

[26] C. Wu, X. Huang, X. Wu, L. Xie, K. Yang, P. Jiang, Graphene oxide-encapsulated carbon nanotube hybrids for high dielectric performance nanocomposites with enhanced energy storage density, Nanoscale 5 (2013) 3847-3855.

[27] H.W. Ha, A. Choudhury, T. Kamal, D.H. Kim, S.Y. Park, Effect of chemical modification of graphene on mechanical, electrical, and thermal properties of polyimide/graphene nanocomposites, ACS Appl. Mater. Interfaces 4 (2012) 4623-4630.

[28] X. Huang, T. Iizuka, P. Jiang, Y. Ohki, T. Tanaka, Role of interface on the thermal conductivity of highly filled dielectric epoxy/AlN composites, J. Phys. Chem. C 116 (2012) 13629-13639.

[29] M. Antunes, V. Realinho, E. Solórzano, M.A. Rodríguez-Pérez, J.A. de Saja, J.I. Velasco, Thermal conductivity of carbon nanofibre-polypropylene composite foams, Def. Diff. Forum 297-301 (2010) 996-1001.

[30] P. Kim, L. Shi, A. Majumdar, P.L. McEuen, Thermal transport measurements of individual multiwalled nanotubes, Phys. Rev. Lett. 87 (2001) 215502.

[31] J. Shen, X. Han, L.J. Lee, Nanoscaled reinforcement of polystyrene foams using carbon nanofibers, J. Cell. Plast. 42 (2006) 105-126.

[32] J. Ling, W. Zhai, W. Feng, B. Shen, J. Zhang, W. Zheng, Facile preparation of lightweight microcellular polyetherimide/graphene composite foams for electromagnetic interference shielding, ACS Appl. Mater. Interfaces 5 (2013) 2677-2684.

[33] B. Shen, W. Zhai, M. Tao, J. Ling, W. Zheng, Lightweight, multifunctional polyetherimide/graphene@Fe3O4 composite foams for shielding of electromagnetic pollution, ACS Appl. Mater. Interfaces 5 (2013) 11383-11391.

[34] G. Gedler, M. Antunes, V. Realinho, J.I. Velasco, Novel polycarbonate-graphene nanocomposite foams prepared by CO_2 dissolution, IOP Conf. Series: Mater. Sci. Eng. 31 (2012) 012008.

[35] C. Forest, P. Chaumont, P. Cassagnau, B. Swoboda, P. Sonntag, Polymer nano-foams for insulating applications prepared from CO_2 foaming, Prog. Polym. Sci. 41 (2015) 122-145.

[36] Eaves D. Handbook of Polymer Foams, Shawbury, UK: Rapra Technology Limited, 2004, p. 189.

[37] M. Antunes, V. Realinho, J.I. Velasco, Study of the influence of the pressure drop rate on the foaming behavior and dynamic-mechanical properties of CO_2 dissolution microcellular polypropylene foams, J. Cell. Plast. 46 (2010) 551-571.

[38] S.K. Goel, E.J. Beckman, Generation of microcellular polymers using supercritical CO_2, Cell. Polym. 12 (1993) 251-274.

[39] K.A. Arora, A.J. Lessor, T.J. McCarthy, Preparation and characterization of microcellular polystyrene foams processed in supercritical carbon dioxide, Macromolecules 31 (1998) 4614-4620.

[40] A. Cooper, Synthesis and processing of polymers using supercritical carbon dioxide, J. Mater. Chem. 10 (2000) 207-234.

[41] P.M. Nam, M. Okamoto, T. Kotaka, T. Nakayama, M. Takada, M. Ohshima, et al., Foam processing and cellular structure of polypropylene/clay nanocomposites, Polym. Eng. Sci. 42 (2002) 1907-1918.

[42] K. Taki, T. Yanagimoto, E. Funami, M. Ohshima, Visual observation of CO_2 foaming of polypropylene-clay nanocomposites, Polym. Eng. Sci. 44 (2004) 1004-1011.

[43] G. Gedler, M. Antunes, J.I. Velasco, Polycarbonate foams with tailor-made cellular structures by controlling the dissolution temperature in a two-step supercritical carbon dioxide foaming process, J. Supercritical Fluids 88 (2014) 66-73.

[44] G. Gedler, M. Antunes, J.I. Velasco, Effects of graphene nanoplatelets on the morphology of polycarbonate-graphene composite foams prepared by supercritical carbon dioxide two-step foaming, J. Supercritical Fluids 100 (2015) 167-174.

[45] G. Sims, C. Khunniteekool, Cell size measurement of polymeric foams, Cell. Polym. 13 (1994) 137-146.

[46] C. T'Joen, Y. Park, Q. Wang, A. Sommers, X. Han, A. Jacobi, A review on polymer heat exchangers for HVAC&R applications, Inter. J. Refrigeration 32 (2009) 763-779.

[47] Gibson L.J., Ashby M.F. Cellular Solids, Structure and Properties. 2nd ed., Oxford: Pergamon Press, 1999.

[48] S. Stankovich, D.A. Dikin, G.H.B. Dommett, K.M. Kohlhaas, E.J. Zimney, E.A. Stach, et al., Graphene-based composite materials, Nature 442 (2006) 282-286.

[49] D. Galpaya, M. Wang, L. Meinan, N. Motta, E. Waclawik, C. Yan, Recent advances in fabrication and characterization of graphene-polymer nanocomposites, Graphene 1 (2012) 30-49.

[50] F. Yavari, H.R. Fard, K. Pashayi, M.A. Rafiee, A. Zamiri, Z. Yu, et al., Enhanced thermal conductivity in a nanostructured phase change composite due to low concentration graphene additives, J. Phys. Chem. C 115 (2011) 8753-8758.

[51] A.A. Balandin, Thermal properties of graphene and nanostructured carbon materials, Nat. Mater. 10 (2011) 569-581.

[52] L. Ren, K. Pashayi, H.R. Fard, S.P. Kotha, T. Borca-Tasciuc, R. Ozisik, Engineering the coefficient of thermal expansion and thermal conductivity of polymers filled with high aspect ratio silica nanofibers, Comp. Part B: Eng. 58 (2014) 228-234.

[53] S. Shenogin, L. Xue, R. Ozisik, P. Keblinski, D.G. Cahill, Role of thermal boundary resistance on the heat flow in carbon-nanotube composites, J. Appl. Phys. 95 (2004) 8136-8144.

[54] G. Gedler, M. Antunes, J.I. Velasco, Graphene-induced crystallinity of bisphenol A polycarbonate in the presence of supercritical carbon dioxide, Polymer 54 (2013) 6389-6398.

[55] G. Gedler, M. Antunes, J.I. Velasco, R. Ozisik, Electromagnetic shielding effectiveness of polycarbonate/graphene nanocomposite foams processed in 2-steps with supercritical carbon dioxide, Mater. Lett. 160 (2015) 41-44.

[56] M. Antunes, J.I. Velasco, Multifunctional polymer foams with carbon nanoparticles, Prog. Polym. Sci. 39 (2014) 486-509.

[57] K. Pashayi, H.R. Fard, F. Lai, S. Iruvanti, J. Plawsky, T. Borca-Tasciuc, High thermal conductivity epoxy-silver composites based on self-constructed nanostructured metallic networks, J. Appl. Phys. 111 (2012) 104310.

[58] Weast R.C. Handbook of Chemistry and Physics, 53rd edition: Chemical Rubber Pub., 1972.

Figure captions

Figure 1. Scheme of the setup used for measuring thermal resistance.

Figure 2. (a) Thermal conductivity as a function of relative density for unfoamed and foamed PC and PC-GnP nanocomposites (X1 and X2 indicate foams that were prepared by 1– and 2–step foaming, respectively). Typical SEM micrographs of the cell strut of: (b) high relative density 1–step foams and (c) low relative density 2–step foams (both with 0.5 wt% GnP). Note: R^2 values corresponding to the linear fittings are indicated for each set of foams.

Figure 3. Normalized thermal conductivity as a function of relative density for unfilled PC and PC-GnP nanocomposite foams.

Figure 4. (a) Thermal conductivity as a function of cell size for unfilled PC and PC-GnP nanocomposite foams prepared via 1– and 2–step foaming. PC-GnP nanocomposites prepared in 1–step followed a linear behaviour while nanocomposites prepared via 2–step foaming showed a more scattered behaviour. Micrographs showing the typical cellular structure of foams prepared by: (b) 1–step (unfilled PC) and (c) 2–step foaming (5 wt% GnP).

Figure 5. Thermal conductivity of PC-GnP nanocomposite foams as a function of graphene volume concentration. The thermal conductivity of unfoamed nanocomposites is indicated using red symbols. Note: R^2 values corresponding to the linear fittings are indicated for each set of foams.

Figure 6. Scheme showing the dispersion/exfoliation of graphene nanoplatelets due to interaction with CO_2 molecules during foaming.

Figure 7. TEM micrographs of graphene nanoparticles present in PC-GnP nanocomposite foams prepared via 1–step foaming: (a) X1PC05 foams exhibited thinner and more close GnP nanoparticles when compared to (b) X1PC2 foams.

Figure 8. Comparison between the experimentally measured thermal conductivities ($k_{experimental}$) and the theoretical thermal conductivities calculated using Model I (black symbols) and Model II (red symbols) of PC-GnP nanocomposite foams.

Table 1. Cellular characteristics of polycarbonate (PC) and polycarbonate-graphene (PC-GnP) nanocomposite foams prepared via 1– and 2–step foaming.

GnP concentration (wt%)	Foaming method	Relative density range	Cell density (cells/cm^3)	ϕ_{VD} (μm)	Aspect ratio
0.0	1–step	0.33–0.46	4.64×10^5–5.51×10^6	159–68	0.8–1.0
	2–step	0.08–0.15	4.96×10^7–3.72×10^8	60–30	0.9–1.3
0.5	1–step	0.34–0.78	1.04×10^6–2.70×10^6	146–73	0.8–1.0
	2–step	0.08–0.28	6.19×10^7–1.56×10^9	46–11	1.0–1.4
2.0	1–step	0.37–0.54	2.07×10^5–7.93×10^5	210–123	0.9–1.1
	2–step	0.18–0.32	3.82×10^7–1.61×10^9	57–26	1.0–1.4
5.0	1–step	0.53–0.83	1.73×10^6–1.18×10^7	50–30	0.8–1.0
	2–step	0.44–0.52	5.60×10^8–1.01×10^9	20–12	1.1–1.5

Relative density, cell density, cell size in the vertical direction (ϕ_{VD}) and aspect ratio, *AR* (*AR* = ϕ_{VD}/ϕ_{WD}) are given as a range of values obtained from foams by using different foaming conditions. Each value represents an average of multiple measurements. Complete set of data is provided in references [34, 43-44].